British Journal of Cancer www.nature.com/bjc

ARTICLE

The KDM6A-SPARCL1 axis blocks metastasis and regulates the tumour microenvironment of gastrointestinal stromal tumours by inhibiting the nuclear translocation of p65

Chaoyong Shen[1,3], Luyin Han[2,3], Baike Liu[1], Guixiang Zhang[1], Zhaolun Cai[1], Xiaonan Yin[1], Yuan Yin[1], Zhixin Chen[1] and Bo Zhang[1]✉

BACKGROUND: It is urgent to explore the pathogenic mechanism of gastrointestinal stromal tumours (GISTs). KDM6A, a histone demethylase, can activate gene transcription and has not been reported in GISTs. SPARCL1 may serve as a metastasis marker in GIST, but the molecular mechanism remains to be further explored. This study aimed to explore the biological function and molecular mechanism of KDM6A and SPARCL1 in GIST.

METHODS: CCK-8, live cell count, colony formation, wound-healing and Transwell migration and invasion assays were employed to detect the cell proliferation, migration and invasion. A xenograft model and hepatic metastasis model were used to assess the role of KDM6A and SPARCL1 in vivo.

RESULTS: KDM6A inhibited the proliferation, migration and invasion of GIST cells. Mechanistically, KDM6A promotes the transcription of SPARCL1 by demethylating histone H3 lysine trimethylation and consequently leads to the inactivation of p65. SPARCL1 affected the metastasis of GIST cells in a mesenchymal-epithelial transition- and matrix-metalloproteinase-dependent manner. SPARCL1 knockdown promoted angiogenesis, M2 polarisation and macrophage recruitment by inhibiting the phosphorylation of p65. Moreover, KDM6A and SPARCL1 inhibited hepatic metastasis and macrophage infiltration in vivo.

CONCLUSIONS: Our findings establish the critical role of the KDM6A-SPARCL1-p65 axis in restraining the malignancy of GIST.

British Journal of Cancer (2022) 126:1457–1469; https://doi.org/10.1038/s41416-022-01728-3

BACKGROUND

A gastrointestinal stromal tumour (GIST) is the most common mesenchymal tumour of the gastrointestinal tract and accounts for ~1–3% of gastrointestinal malignancies [1–3]. GISTs frequently occur in the stomach followed by the small intestine and rarely occur in the colon/rectum and the oesophagus [4]. High-risk GISTs are prone to metastasis and can easily grow from a small stromal tumour with benign behaviour to a tumour with highly malignant biological behaviour [3, 5]. GISTs are a heterogeneous group of tumours with harbour mutually exclusive KIT or PDGFRA gain-of-function mutations [1]. GISTs are resistant to standard cytotoxic treatments used for other sarcomas, but tyrosine kinase inhibitors (TKIs) that target KIT and/or PDGFRA significantly improved patient survival [3, 6]. However, another challenge is a lack of effective therapy for GIST when the abovementioned genes are not mutated. Therefore, it is important to explore the disease mechanisms and consider new therapeutic approaches for GIST.

Histone modifications are a significant mechanism for the regulation of gene transcription [7]. Lysine demethylase 6 A (KDM6A) is a member of the JmjC domain-containing enzyme family and regulates the demethylation of H3K27me2/3, therefore leading to transcriptional activation [8, 9]. Deleterious mutations in KDM6A are found in many cancer types, including bladder cancer [9], breast cancer [10, 11] and T-cell acute lymphoblastic leukaemia [12]. KDM6A inhibited the motility and invasiveness of bladder cancer cells [9]. KDM6A enhances tumour immune cell recruitment, promotes differentiation and suppresses medulloblastoma [13]. KDM6A participates in the imatinib resistance in chronic myelogenous leukaemia [14]. Moreover, KDM6A has also been reported to play an oncogenic role in non-small-cell lung cancer by regulating H3K4me3 [15]. However, the role of KDM6A in GIST has not yet been reported.

SPARCL1 (secreted protein acidic and rich in cysteine like protein 1) is an extracellular matrix glycoprotein, belonging to the SPARC family of stromal cell proteins [16]. It is related to the regulation of cell adhesion, migration and proliferation. SPARCL1 is expressed in physiological environments, including embryogenesis and adult tissue remodelling. However, compared with the widespread expression in normal tissues, SPARCL1 has been found to be downregulated in many human epithelial cancers, such as non-small-cell lung cancer, prostate cancer, pancreatic cancer and colon cancer, suggesting that SPARCL1 may play a role as a tumour suppressor [17]. In addition, some reports show that SPARCL1 inhibits the migration and invasion of prostate cancer and colorectal cancer cells in vitro and in vivo [18, 19]. SPARCL1, as a matrix protein, is an important part of the microenvironment. It has been reported that SPARCL1 can participate in the regulation of metastasis of prostate cancer [20] and vascular homeostasis in

[1]Department of Gastrointestinal Surgery, West China Hospital, Sichuan University, 610041 Chengdu, Sichuan, China. [2]Intensive care unit, West China Hospital, Sichuan University, 610041 Chengdu, Sichuan, China. [3]These authors contributed equally: Chaoyong Shen, Luyin Han. ✉email: hxwcwk@126.com

Received: 22 June 2021 Revised: 7 January 2022 Accepted: 28 January 2022
Published online: 8 February 2022

colorectal cancer [21] by remodelling the tumour microenvironment. Our previous study found that SPARCL1 was expressed at low levels in GIST tissue and has potential diagnostic value for GIST [22]. Moreover, the expression of SPARCL1 is closely related to the malignant degree of GIST. The knockdown of SPARCL1 had no significant effect on the cell viability, cell cycle or apoptosis of GIST-882 cells. However, SPARCL1 knockdown significantly increased the migration and invasion ability of GIST-882 cells. We also found that the knockdown of SPARCL1 could significantly promote the liver metastasis of GIST-882 in vivo. However, the molecular mechanism by which SPARCL1 regulates GIST remains to be further explored.

In the current study, we identified that KDM6A and SPARCL1 were markedly downregulated in GIST patients. KDM6A promoted SPARCL1 transcription by directly demethylating H3K27 at the SPARCL1 promoter. The activation of the p65 signaling pathway was induced by SPARCL1 knockdown, which led to angiogenesis and tumour-associated macrophage recruitment, ultimately contributing to GIST metastasis.

MATERIALS AND METHODS

Tissue specimens

Patients who underwent surgery at West China Hospital in the period from February 2015 to March 2021 were the source of the 48 GIST samples used in this study. The samples were subjected to snap freezing in liquid nitrogen and stored at −80 °C. HE staining was used by two pathologists to pathologically confirm the samples. Informed consent was provided by each patient, and the protocol of this study was approved by the Research Ethics Board of West China Hospital, Sichuan University.

Cell culture

The monocyte cell line, THP-1 and the human GIST cell lines, GIST-882 and GIST-T1 were purchased from the BeNa Culture Collection (Beijing, China) and were checked and authenticated for genotypes by DNA fingerprinting within 6 months. All cells were cultured in Dulbecco's modified Eagle's medium (Gibco, Grand Island, NY, USA) supplemented with 10% fetal bovine serum (Gibco), penicillin (100 U/mL; Invitrogen, USA) and streptomycin (100 μg/mL; Invitrogen, USA). The monocyte THP-1 cells were induced with 50 ng/mL phorbol-12-myristate-13-acetate (PMA, Sigma–Aldrich, USA) for 72 h to adhere and generate THP-1-derived macrophages.

Cell transfection

The overexpression vector for KDM6A, EZH2 and SPARCL1 and shRNA for KDM6A and SPARCL1 were all obtained from GenePharma (Shanghai, China). Transfection was performed using Lipofectamine 2000 (Invitrogen, Carlsbad, CA, USA) according to the manufacturer's instructions.

Nuclear and cytoplasmic protein extraction and western blot

Nuclear and cytoplasmic proteins were obtained using the Nuclear and Cytoplasmic Protein Extraction Kit (Beyotime, Beijing, China). Total protein was extracted using RIPA buffer on ice. The extracts were loaded onto SDS polyacrylamide gels, electrophoresed and blotted onto PVDF membranes. After blocking with 5% skimmed milk, the membrane was incubated with primary antibodies and secondary antibodies. Then, the bands were detected using an ECL kit (Beyotime). All antibodies were obtained from Cell Signaling Technology (Danvers, USA).

RNA isolation and quantitative real-time PCR

Total RNA was extracted using TRIzol (Invitrogen, Carlsbad, CA). One microgram of RNA was used to generate cDNA using the High-Capacity cDNA Reverse Transcription kit (Applied Biosystems, Foster City, CA). Real-time quantitative PCR (qRT-PCR) was performed using the ABI7900HT Fast Real-Time PCR system (Applied Biosystems). The qRT-PCR primers used were purchased from Sangon Biotech, and the primer sequences are shown in Supplementary Table S1.

ChIP assays

Chromatin immunoprecipitation (ChIP) was performed using a Simple ChIP Enzymatic Chromatin IP Kit (Cell Signaling Technology) and followed the kit protocol. Briefly, the cells were crosslinked with 1% formaldehyde. The DNA and proteins were broken down by ultrasonic shearing. The supernatant was incubated with antibodies and the DNA in the complexes was extracted and detected by PCR.

Assay for cell proliferation

For the CCK-8 assay, 20 μl of CCK-8 was added to each well at 37 °C for 2 h. The optical density (OD) was measured using absorbance at 450 nm at various time points: 0, 24, 48 and 72 h.

For the live cell count assay, 10k cells per well were seeded in six-well plates for 72 h. Then the cells were harvested and centrifuged. The pellets were incubated with a 0.04% Trypan blue (Euro Clone, West York, UK) solution for 5 min to analyze the cell number. The cells were transferred to a Bürker counting chamber and then counted by microscopy.

For the colony formation assay, 3k cells per well were seeded in 6-well plates and cultured at 37 °C for 7–14 d. The cell colonies were stained with crystal violet and counted.

Wound-healing and transwell assays

For the wound-healing assay, GIST cells were plated to form a full monolayer. A wound was created by scratching with a 200 μL pipette tip, and the intercellular distance was measured at 0 h and 24 h. The wound-healing ratio was calculated as follows; migration distance/primary intercellular distance × 100%.

For the Transwell migration assay, 50k cells in 200 μL serum-free medium were plated onto a Transwell chamber containing a polycarbonate membrane with 8.0 μm pores. The chamber was placed in a 24-well plate containing 600 μL medium with 10% fetal bovine serum. After incubation at 37 °C for 48 h, the cells on the upper membrane surface were mechanically removed. Migrated cells were counted after fixation in 4% paraformaldehyde for 20 min and dyed with 0.1% crystal violet staining solution (Beyotime) for 10 min.

For the Transwell invasion assay, the polycarbonate membrane was covered with a layer of Matrigel matrix and the following steps were the same as those in the Transwell migration assay.

Assay for endothelial cell tube formation

GIST cell lines were indicated overnight and the conditioned medium was collected. HUVECs (20 k per well) were seeded into 96-well plates with Matrigel along with the above-described conditioned medium. After incubation, tube formation was detected by microscopy, and the branch number and tube length in the formed HUVEC tubes were quantified.

Flow cytometry

Cells were collected, washed, and incubated for 30 min at 4 °C with florescence-conjugated antibodies (CD206 and CD86). Labelled cells were analyzed using a flow cytometer (BD, San Jose, CA) and FlowJo software (Tree Star Inc., Oregon, USA).

Macrophage chemotaxis assays

GIST cells were seeded into the lower compartment of an 8.0-μm-pore Transwell system. THP-1 cells were overlaid onto the upper chamber. After incubation for 24 h, the migrated macrophages were stained with crystal violet and counted.

Tumour xenograft models

All animal experiments were conducted under an approved protocol from the Sichuan University Institutional Animal Care and Use Committee. Five-week-old female BALB/c (nu/nu) mice were purchased from Vital River Laboratory Animal Technology Co. Ltd. and raised under specific pathogen-free conditions.

For the subcutaneous tumour model, 1×10^6 GIST-882 cells were injected subcutaneously into the axillary fossa of each mouse. Each group was randomly assigned 7 mice. The volume of tumour nodules was measured every 7 days, and mice were sacrificed 28 d after implantation. The tumour nodules were excised, weighed and embedded in paraffin for immunohistochemistry and immunofluorescence. Blinding was employed for this experiment.

For the hepatic metastasis mouse model, a middle abdominal incision was carried out to expose the spleen. Each group was randomly assigned seven mice. A total of 1×10^7 viable tumour cells were implanted into the splenic subcapsular space, the spleen was excised completely, and the

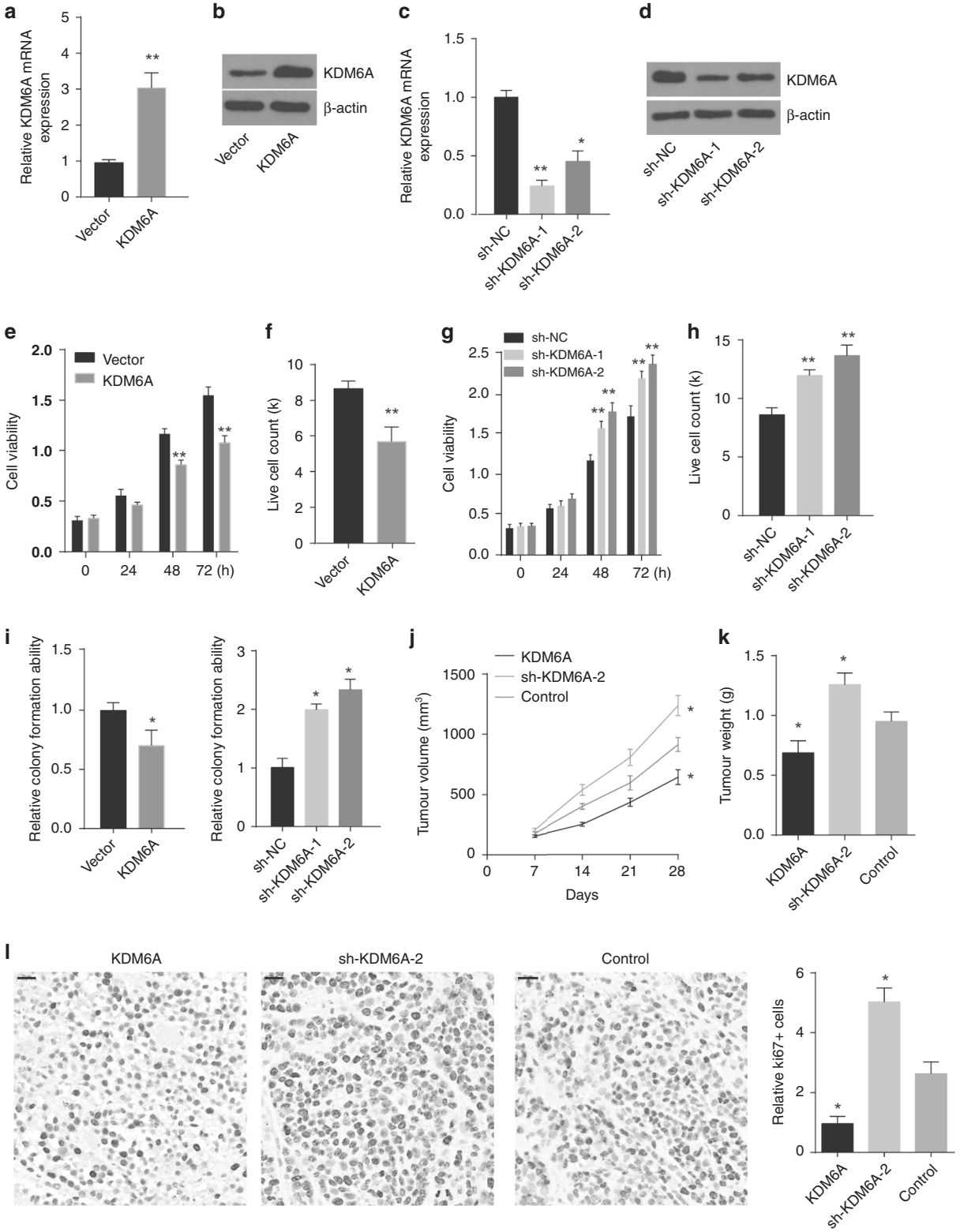

abdominal incision was stitched. The mice were euthanised on Day 30 post-injection. The liver was collected and fixed in 10% formalin. Metastatic nodules were identified by colour and appearance and counted under a dissecting microscope. Metastatic liver nodules were further confirmed via hematoxylin and eosin (H&E) staining. Blinding was employed for this experiment.

Statistical analysis

The results were displayed as the mean ± SD or SEM. Two-tailed Student's *t*-test and one-way analysis of variance (ANOVA) followed by Tukey's test were used to compare the differences in two groups and multiple groups. $P < 0.05$ was considered statistically significant. Three biological or technological replicates were performed for each experiment.

Fig. 1 KDM6A inhibits GIST-882 cell growth. a, b Lentivirus-mediated KDM6A overexpression in GIST-882 cells was examined by qRT-PCR and western blot. $^{**}P < 0.01$ vs. vector. **c, d** Lentivirus-mediated KDM6A knockdown in GIST-882 cells was detected by qRT-PCR and western blot. $^{*}P < 0.05$, $^{**}P < 0.01$ vs. sh-NC. **e** The viability of GIST-882 cells stably expressing vector or KDM6A was detected by CCK-8 assay. $^{**}P < 0.01$ vs. vector. **f** The effect of KDM6A overexpression on GIST-882 cell proliferation was examined by live cell count. $^{**}P < 0.01$ vs. vector. **g** The effect of KDM6A knockdown on the viability of GIST-882 cells was detected by CCK-8 assay. $^{**}P < 0.01$ vs. sh-NC. **h** The effect of KDM6A knockdown on GIST-882 cell proliferation was examined by live cell count. $^{**}P < 0.01$ vs. sh-NC. **i** Colony formation assays were performed to verify the role of KDM6A in GIST-882 cell colony formation. $^{*}P < 0.05$ vs. vector or sh-NC. **j** GIST-882 control vector cells, KDM6A overexpression cells or KDM6A knockdown cells were subcutaneously injected into BALB/c nude mice. Tumour volume growth curves are presented. $^{*}P < 0.05$ vs. control group. Data were displayed as the mean ± SEM. **k** After 28 days, mice were sacrificed, and tumour weights were examined. $^{*}P < 0.05$ vs. control. Data were displayed as the mean ± SEM. **l** Representative IHC staining of Ki-67 is presented. Scale bar: 20 μm. $^{*}P < 0.05$ vs. control. Data were displayed as the mean ± SEM.

RESULTS

KDM6A inhibits GIST cell growth in vitro and in vivo

To explore the function of KDM6A in GIST, KDM6A overexpression vector or shRNA vectors were transfected into GIST-882 cell lines. As shown in Fig. 1a, b, transfection of KDM6A overexpression vector raised the mRNA levels and the protein expression of KDM6A in both GIST-882 cells. The transfection of both shRNA vectors of KDM6A decreased the mRNA levels and protein expression of KDM6A in GIST-882 cells (Fig. 1c, d). KDM6A overexpression inhibited the viability of GIST-882 cells (Fig. 1e). The results of the live cell count assay also indicated that KDM6A inhibited the proliferation of GIST-882 cells (Fig. 1f). Consistently, KDM6A knockdown enhanced the viability and proliferation of GIST-882 cells (Fig. 1g, h). Moreover, colony formation assays showed higher numbers of colonies in the cells of colonies in the KDM6A knockdown group and fewer colonies in the KDM6A overexpression group (Fig. 1i). Consistently, KDM6A overexpression also inhibited the viability, proliferation and colony formation of GIST-T1 cells (Supplementary Fig. S1A-F) and KDM6A downregulation promoted the viability, proliferation and colony formation of GIST-T1 cells (Supplementary Fig. S1G-J). These results are indicative of KDM6A restraining the proliferation and colony formation of GIST cells in vitro.

To evaluate the role of KDM6A in tumour growth in vivo, GIST-882 cells overexpressing or knocking down KDM6A were employed to construct tumour xenograft models. After implantation, both the volume and weight of the tumours were decreased after KDM6A overexpression and were increased after KDM6A knockdown (Fig. 1j, k). Moreover, the results of the immunohistochemical staining of Ki-67 indicated that there were fewer Ki-67 positive cells in KDM6A overexpressing tumour xenografts and more Ki-67 positive cells in tumour xenografts after KDM6A knockdown (Fig. 1l). In short, KDM6A regulates GIST-882 cell proliferation and progression in vivo.

KDM6A inhibits the migration and invasion of GIST cells in vitro and metastasis in vivo

As GIST therapy is hindered by metastasis at a clinical level, we further explored the role of KDM6A in metastasis. Wound-healing assays showed that the KDM6A overexpression significantly inhibited wound-healing and that KDM6A knockdown promoted wound-healing in both GIST-882 (Fig. 2a) and GIST-T1 cells (Supplementary Fig. S2A). Transwell migration and Transwell invasion assays indicated that KDM6A overexpression reduced the cell migration and invasion ability (Fig. 2b, c). KDM6A knockdown increased the cell migration and invasion ability of GIST-882 (Fig. 2b, c) and GIST-T1 cells (Supplementary Fig. S2B-C). Because the liver is the most common metastatic site of GISTs, the intrasplenic implantation was conducted to assess the influence of KDM6A on hepatic metastasis. Metastatic nodule formation was significantly increased in the KDM6A knockdown groups and KDM6A overexpression reduced the metastatic nodule formation of GIST-882 cells in vivo (Fig. 2d, e). These results demonstrate that KDM6A influences the development of hepatic metastasis of GIST cells in vivo.

Epithelial–mesenchymal transition (EMT) and its reverse process, mesenchymal-epithelial transition (MET), are recognised as critical events for the tumour progression and metastasis of carcinomas [23, 24]. We next examined the influence of KDM6A on MET related gene expression. KDM6A overexpression reduced the mRNA levels of N-cadherin, vimentin, Snail, Twists and ZEBs and enhanced the mRNA levels of E-cadherin in GIST-882 (Fig. 2f) and GIST-T1 (Supplementary Fig. S2D) cells. Meanwhile, KDM6A knockdown decreased E-cadherin mRNA levels and increased mRNA levels of N-cadherin, vimentin, Snail, Twists and ZEBs in GIST-882 and GIST-T1 cells. In addition, KDM6A overexpression reduced the mRNA levels of MMP2 and MMP9 and KDM6A knockdown increased MMP2 and MMP9 mRNA levels in GIST-882 (Fig. 2g) and GIST-T1 cells (Supplementary Fig. S2E). These data suggest that KDM6A inhibits the migration and invasion of GIST cells in a MET- and MMP-dependent manner.

Identification of SPARCL1 as a target of KDM6A in GIST

Next, we analysed the potential target genes of KDM6A. Previous studies have shown that SPARCL1 is downregulated in GISTs (Fig. 3a) and that the downregulation of SPARCL1 promotes GIST-882 cell migration and invasion in vitro and enhances liver metastasis in vivo [22]. EZH2 acts as a methyltransferase that catalyzes the methylation of H3K27 to repress gene activation and KDM6A removes the trimethylation mark on H3K27me3 to promote gene activation [25, 26]. According to the ChIP-seq data in the ENCODE database (https://www.encodeproject.org/), we found that KDM6A, EZH2 and H3K27me3 proteins were enriched in SPARCL1 promoter regions, which suggests that KDM6A and EZH2 may be epigenetic regulators for SPARCL1 transcription. To further verify the potential regulatory relationships among KDM6A, EZH2 and SPARCL1, 48 GIST tissues and adjacent normal tissues were collected. In this study, EZH2 was found to be upregulated and KDM6A was found to be downregulated in GISTs (Fig. 3b, c). Subsequently, correlation analysis was employed to verify the correlation among SPARCL1, KDM6A and EZH2. The results revealed that EZH2 expression showed a negative correlation with SPARCL1 or KDM6A in GISTs and that KDM6A expression showed a positive correlation with SPARCL1 in GISTs (Fig. 3d–f). Immunochemistry staining showed a significant SPARCL1 downregulation and KDM6A downregulation in GIST tissues (Fig. 3g, h). SPARCL1 was mainly located in the cytoplasm while KDM6A was mainly located in the nucleus. Furthermore, we also found that EZH2 was upregulated in GIST tissues and was mainly located in the nucleus (Fig. 3i). In the ROC curve, the AUC for EZH2 was 0.858, that for KDM6A was 0.698 and that for SPARCL1 was 0.834. Thus, EZH2, KDM6A and SPARCL1 may serve as diagnostic markers for GIST (Fig. 3j–l). Moreover, analysis of the clinical characteristics of KDM6A suggested that KDM6A expression levels were related to risk classification, mitosis and metastatic recurrence and had no correlation with age, sex, or necrosis (Supplementary Table S2). Similarly, SPARCL1 expression was also found to be related to risk classification, mitosis and metastatic recurrence (Supplementary Table S3).

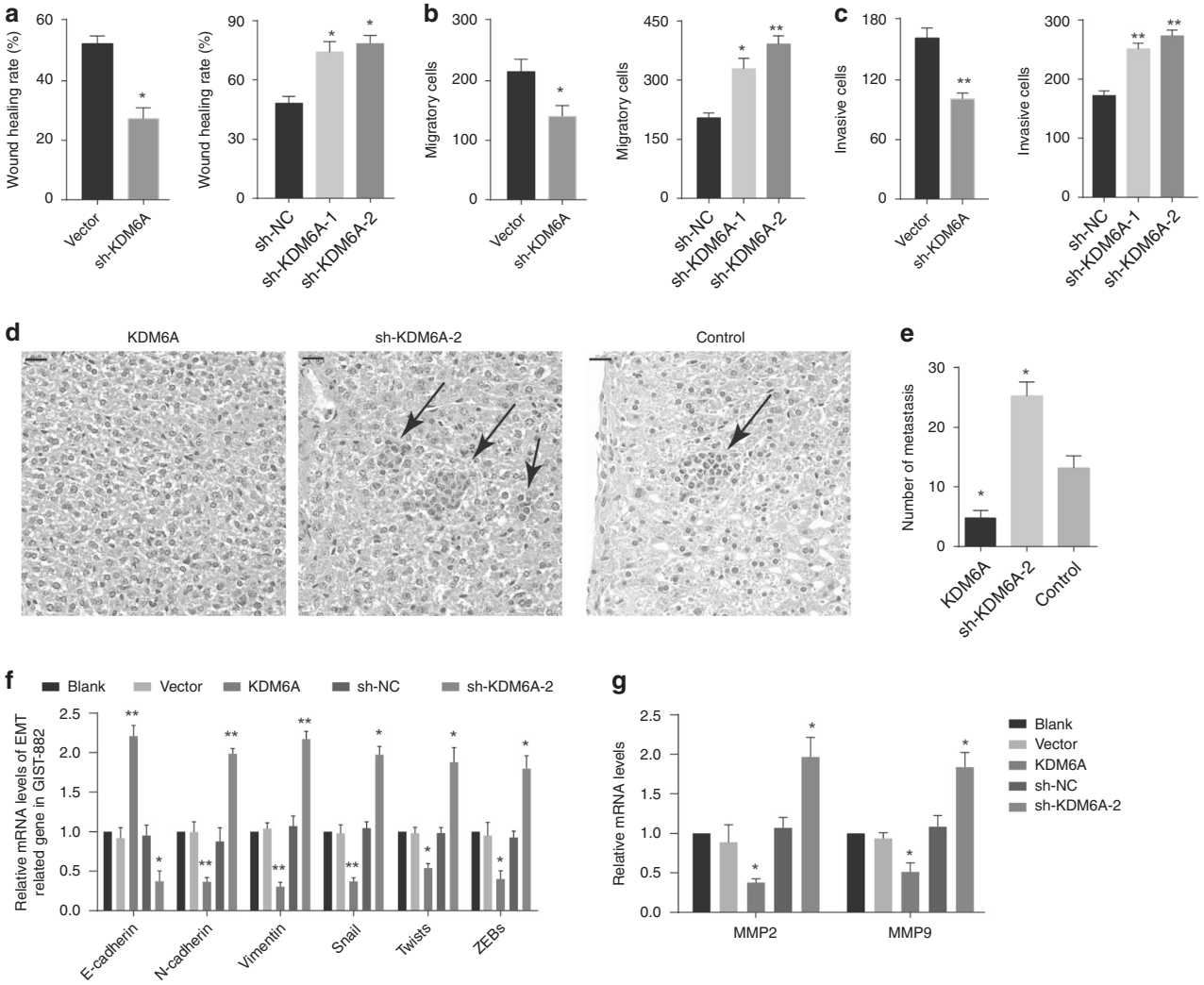

Fig. 2 KDM6A inhibits GIST cell migration, invasion and metastasis. a–c Migration and invasion capacities of GIST-882 cells were examined by wound-healing assays, Transwell migration assays and Transwell invasion assays. *$P < 0.05$, **$P < 0.01$ vs. vector or sh-NC. **d** GIST-882 cells with KDM6A overexpression or knockdown were employed to establish a hepatic metastasis mouse model. Hematoxylin-eosin staining of livers from sacrificed mice is shown. Scale bar: 20 μm. **e** The numbers of metastatic nodules in the livers. *$P < 0.05$ vs. control. Data were displayed as the mean ± SEM. **f** The mRNA levels of E-cadherin, N-cadherin, Snail, vimentin, Twists and ZEBs in GIST-882 cells were examined by qRT-PCR. *$P < 0.05$, **$P < 0.01$ vs. vector or sh-NC. **g** The mRNA levels of MMP2 and MMP9 in GIST-882 cells. *$P < 0.05$ vs. vector or sh-NC.

KDM6A, serving as a histone demethylase, activates gene transcription by antagonising EZH2 through the removal of methyl groups from H3K27 [9, 27]. In the present study, KDM6A overexpression enhanced the protein level of KDM6A and decreased the protein level of H3K27me3 in GIST-882 and GIST-T1 cells (Fig. 4a, b). KDM6A knockdown significantly decreased the protein level of KDM6A and increased the protein level of H3K27me3 in GIST-882 and GIST-T1 cells (Fig. 4a, b). However, the dysregulation of KDM6A in GISTs had no effect on H3 protein levels. To further address the specific regulatory mechanisms between KDM6A and SPARCL1, we performed chromatin immunoprecipitation assays. There was a strong enrichment of KDM6A, EZH2 and H3K27me3 in SPARCL1 promoter regions in both GIST-882 and GIST-T1 cells (Fig. 4c–e). Moreover, we found that KDM6A overexpression enhanced the mRNA and protein levels of SPARCL1 (Fig. 4f, g). Importantly, we determined that EZH2 was also involved in SPARCL1 regulation and found that EZH2 overexpression decreased the mRNA and protein levels of SPARCL1. EZH2 overexpression reversed the stimulation of SPARCL1 induced by KDM6A (Fig. 4f, g). Furthermore, the enrichment of KDM6A was increased, while the enrichment of EZH2 and H3K27me3 was significantly decreased in the SPARCL1 promoter region after KDM6A overexpression in both GIST-882 and GIST-T1 cells (Fig. 4h, i). In contrast, EZH2 overexpression decreased the enrichment of KDM6A, while enhancing the enrichment of EZH2 and H3K27me3 in the SPARCL1 promoter region in both GIST-882 and GIST-T1 cells. EZH2 and KDM6A were epigenetic modifiers with antagonism (Fig. 4h, i). All these results indicate that KDM6A promotes SPARCL1 transcription by directly binding to and demethylating H3K27 at the SPARCL1 promoter.

SPARCL1 restores the promotion of cell migration and invasion induced by KDM6A knockdown

To evaluate the role of SPARCL1 in the biological function of GIST cells mediated by KDM6A, the gain- and loss-of-function studies were performed. Cell counting kit-8 and colony formation assays revealed that KDM6A knockdown promoted the proliferation and clonal formation of GIST cells. However, SPARCL1 overexpression had no effect on the proliferation and clonal formation of GIST-882 (Fig. 5a, b) and GIST-T1 (Supplementary Fig. S3A-B) cells. Wound-healing, Transwell migration and Transwell invasion assays indicated that SPARCL1 overexpression

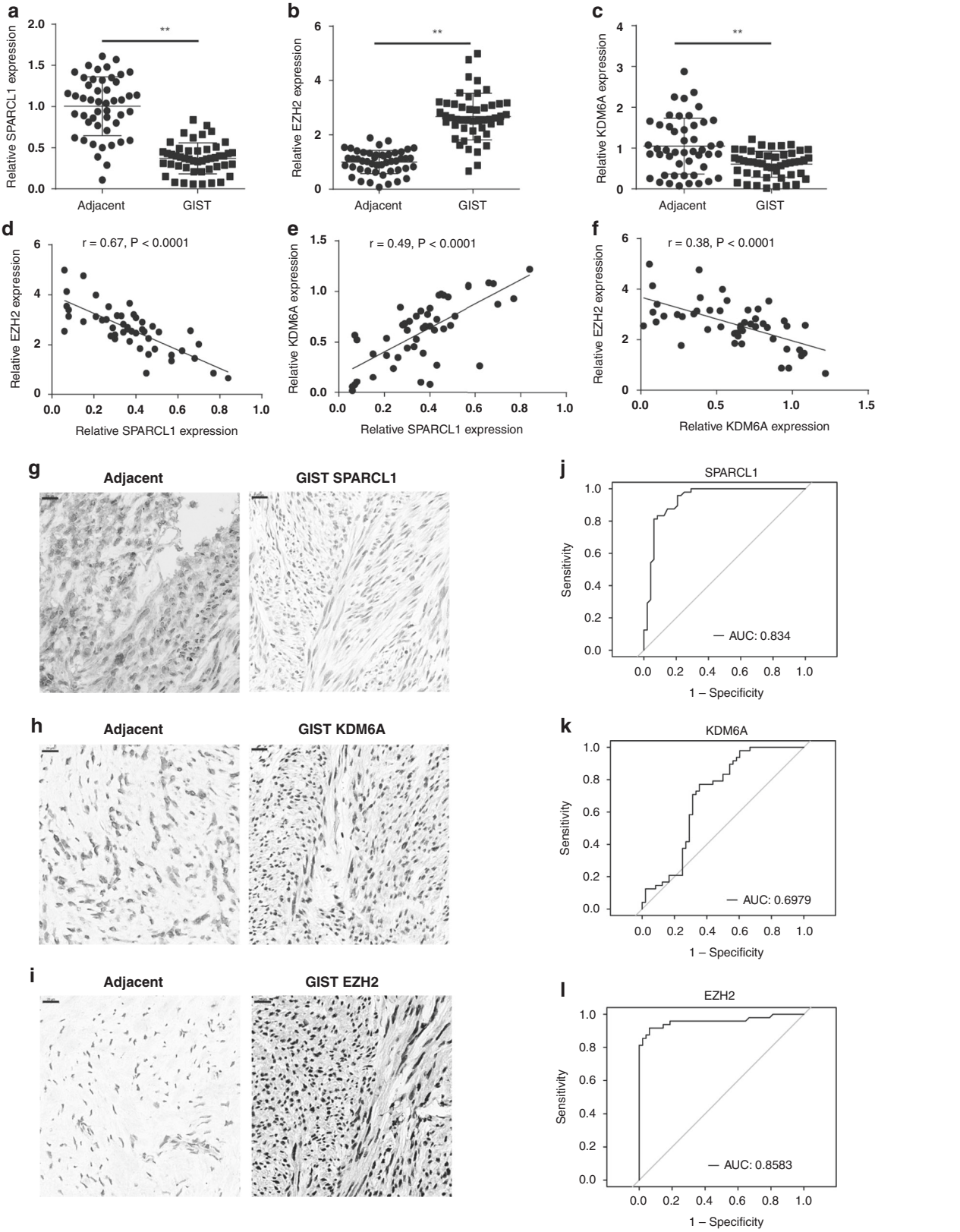

Fig. 3 KDM6A is downregulated in GIST tissues. a–c The mRNA levels of SPARCL1, EZH2 and KDM6A in GIST tissues and adjacent normal tissues were examined by qRT-PCR. $^{**}P < 0.01$. **d–f** The correlation among SPARCL1, EZH2 and KDM6A mRNA levels in 48 GIST tissues was assessed by Spearman's correlation analysis. **g** Representative immunohistochemical staining of SPARCL1 in gastric GISTs. Scale bar: 20 μm. **h** Representative immunohistochemical staining of KDM6A in gastric GISTs. Scale bar: 20 μm. **i** Representative immunohistochemical staining of EZH2 in gastric GISTs. Scale bar: 20 μm. **j–l** ROC curve for SPARCL1, EZH2 and KDM6A was shown.

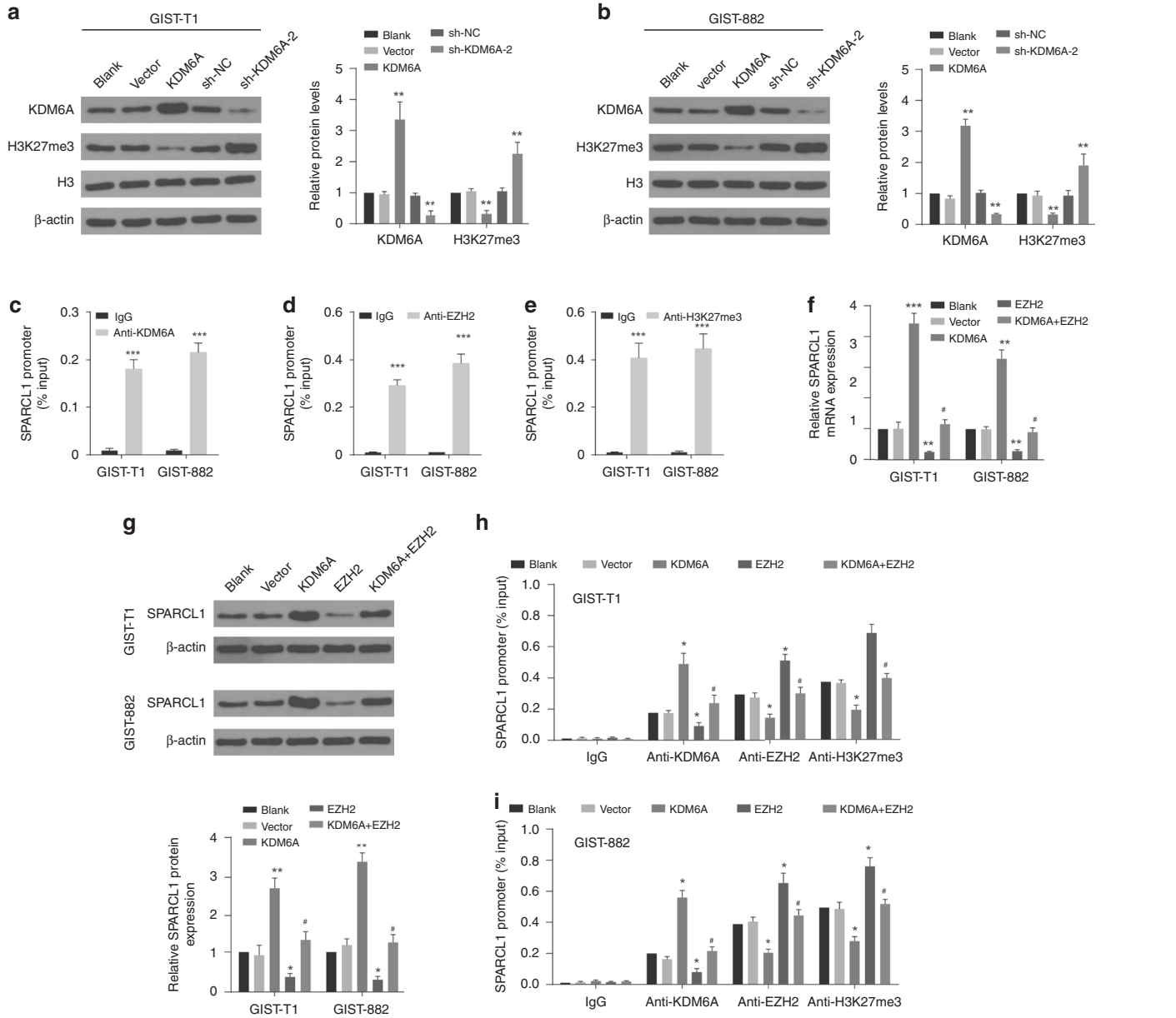

Fig. 4 SPARCL1 is a target of KDM6A. a, b Effect of KDM6A overexpression or knockdown on total H3K27me3 and H3 expression in GIST-882 and GIST-T1 cells. $^{**}P < 0.01$, vs. vector or sh-NC group. **c–e** The enrichment of KDM6A, EZH2 and H3K27me3 in SPARCL1 promoter region was measured by chromatin immunoprecipitation assays. $^{***}P < 0.001$ vs. IgG. **f** The effect of KDM6A or EZH2 overexpression on SPARCL1 mRNA expression. $^{**}P < 0.01$, $^{***}P < 0.001$ vs. vector; $^{\#}P < 0.05$ vs. KDM6A. **g** The effect of KDM6A or EZH2 overexpression on SPARCL1 protein levels. $^{*}P < 0.05$, $^{**}P < 0.05$ vs. vector; $^{\#}P < 0.05$ vs. KDM6A. **h–i** The enrichment of KDM6A, EZH2 and H3K27me3 in SPARCL1 promoter region after KDM6A or EZH2 overexpression was measured by chromatin immunoprecipitation assays. $^{*}P < 0.05$ vs. vector; $^{\#}P < 0.05$ vs. KDM6A.

significantly inhibited the migration and invasion of GIST-882 (Fig. 5c–e) and GIST-T1 (Supplementary Fig. S3C-E) cells. SPARCL1 overexpression restored the promotion induced by KDM6A knockdown on the migration and invasion of GIST-882 (Fig. 5c±e) and GIST-T1 (Supplementary Fig. S3C-E) cells. Moreover, the results of hepatic metastasis mouse models also indicated that SPARCL1 overexpression inhibited metastatic nodule formation and SPARCL1 overexpression reversed metastasis induced by KDM6A knockdown in vivo (Fig. 5f, g). SPARCL1 overexpression reduced the mRNA levels of N-cadherin, vimentin, Snail, MMP2 and MMP9 and enhanced E-cadherin mRNA levels in GIST-882 (Fig. 5h, i) and GIST-T1 (Supplementary Fig. S3F-G) cells. SPARCL1 overexpression played the opposite role in KDM6A knockdown. In short, SPARCL1 acts as a downstream effector of KDM6A to mediate the inhibition of cell migration and invasion in vitro and hepatic metastasis in vivo.

SPARCL1 regulates p65 phosphorylation and allocates its nuclear translocation

We next explored the potential mechanism for SPARCL1 in GIST cell lines. In our work, we found that SPARCL1 knockdown promoted p65 phosphorylation and that SPARCL1 overexpression inhibited p65 phosphorylation in GIST-882 and GIST-T1 cells (Fig. 6a). Both SPARCL1 knockdown and overexpression had no influence on total p65 protein levels. Moreover, SPARCL1 knockdown promoted p65 translocation to the nucleus and SPARCL1 overexpression inhibited p65 translocation to the nucleus in GIST-882 and GIST-T1 cells (Fig. 6b). Furthermore, the phosphorylation of p65 was upregulated

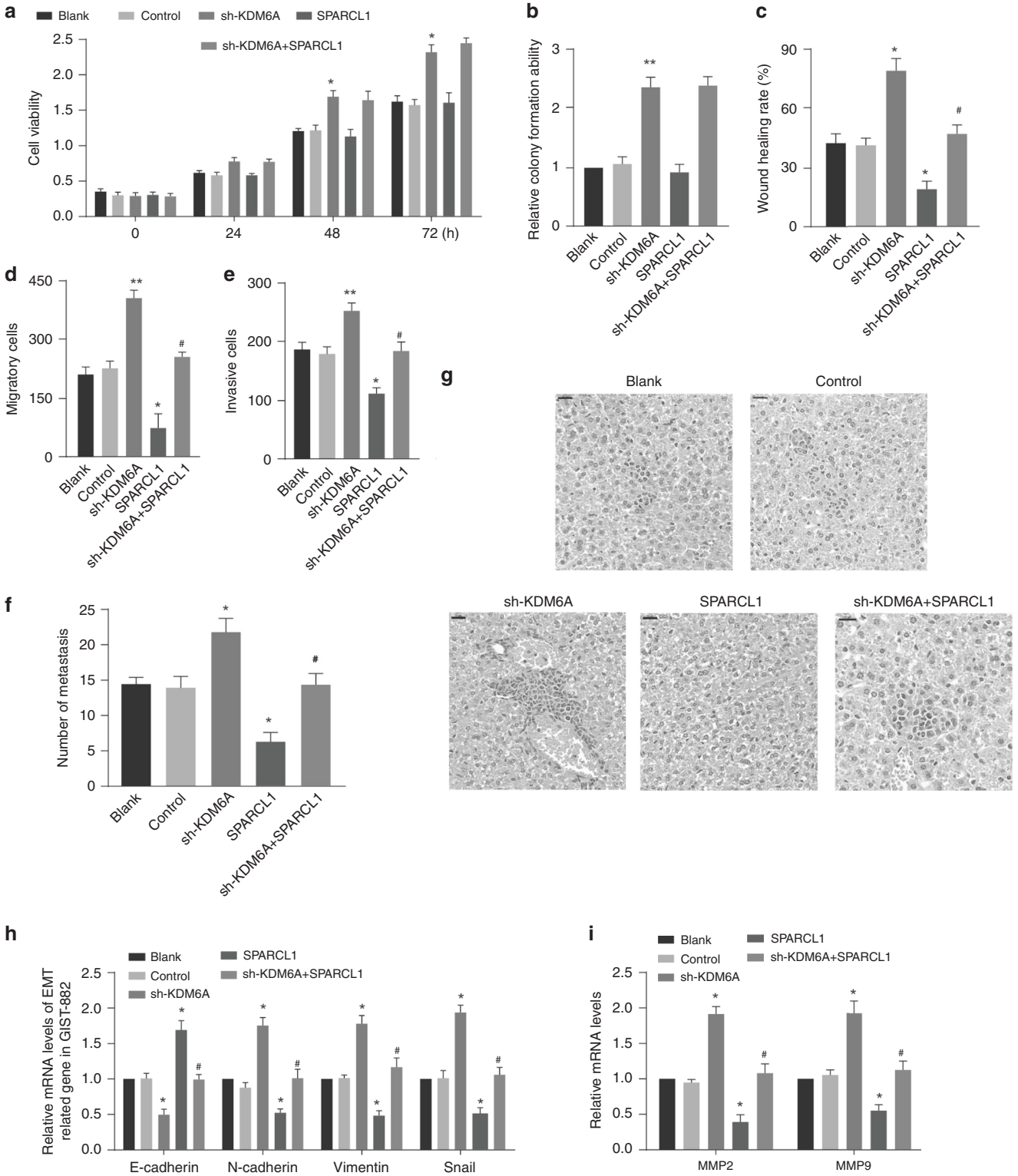

Fig. 5 KDM6A regulates GIST cell migration and invasion by targeting SPARCL1. a The cell viability of GIST-882 cells with the indicated transfection. $^{*}P < 0.05$ vs. control. **b** Colony formation ability of GIST-882 after the indicated transfection. $^{*}P < 0.05$, $^{**}P < 0.01$ vs. control. **c–e** Migration and invasion capacities of GIST-882 cells after the indicated transfection were examined by wound-healing assays, Transwell migration assays and Transwell invasion assays. $^{*}P < 0.05$, $^{**}P < 0.01$ vs. control. $^{\#}P < 0.05$ vs. sh-KDM6A. **f** GIST-882 cells with KDM6A knockdown or SPARCL1 overexpression were employed to establish a hepatic metastasis mouse model. The numbers of metastatic nodules in the livers were shown. $^{*}P < 0.05$ vs. control. $^{\#}P < 0.05$ vs. sh-KDM6A. **g** Hematoxylin-eosin staining of liver from sacrificed mice are shown. Scale bar: 20 μm. Data were displayed as the mean ± SEM. **h** The mRNA levels of E-cadherin, N-cadherin, Snail and vimentin in GIST-882 cells after the indicated transfection were examined by qRT-PCR. $^{*}P < 0.05$ vs. control. $^{\#}P < 0.05$ vs. sh-KDM6A. **i** The mRNA levels of MMP2 and MMP9 in GIST-882 cells after the indicated transfection were examined by qRT-PCR. $^{*}P < 0.05$ vs. control. $^{\#}P < 0.05$ vs. sh-KDM6A.

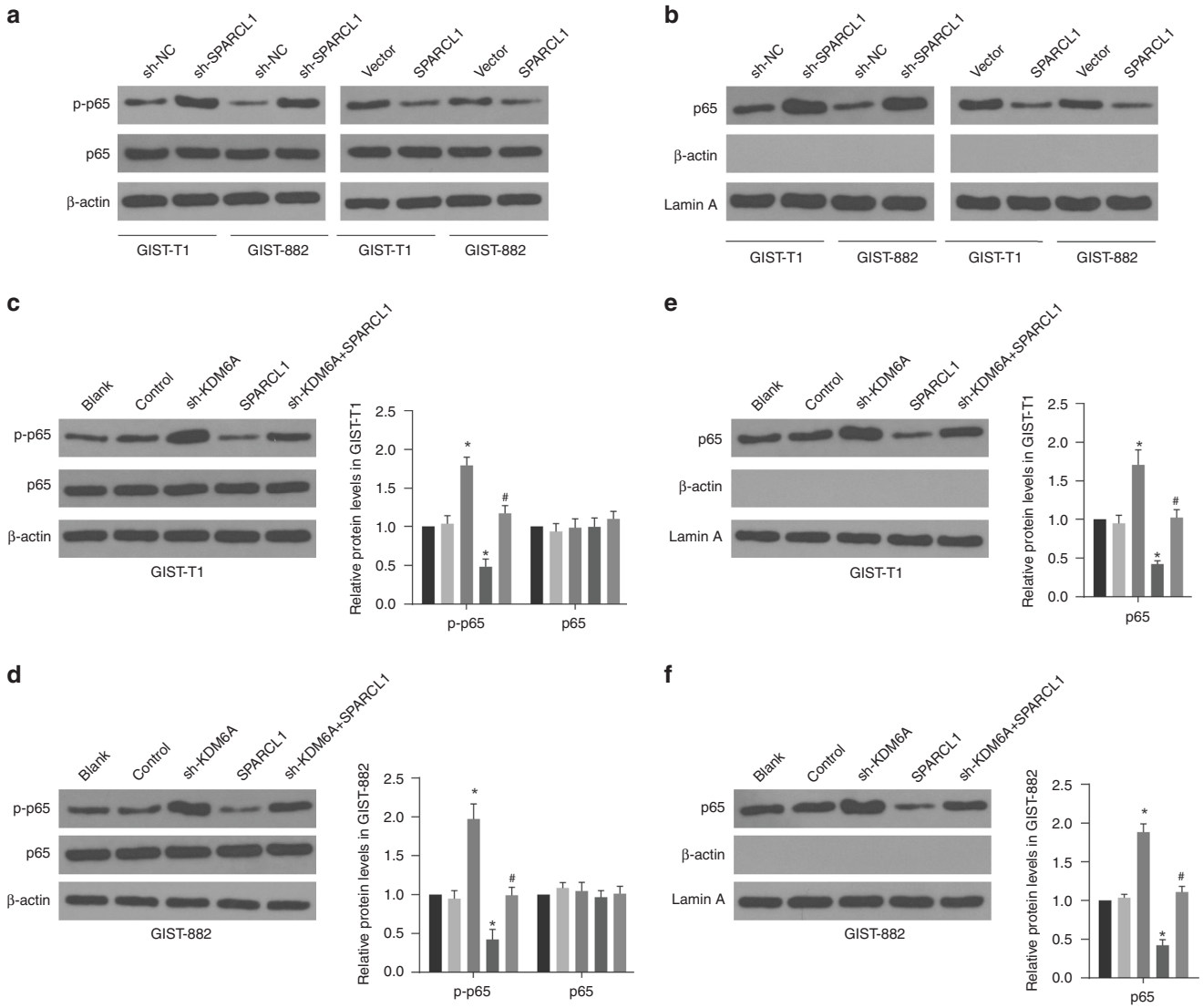

Fig. 6 SPARCL1 regulates p65 phosphorylation and allocates its nuclear translocation. a The phosphorylation of p65 was analyzed in GIST-882 and GIST-T1 cells after SPARCL1 overexpression or knockdown by western blotting. **b** Nuclear fractions were isolated from GIST-882 and GIST-T1 cells after SPARCL1 overexpression or knockdown and analyzed for p65 expression by western blotting. Lamin A and β-actin were used as controls for loading and fractionation. **c, d** The phosphorylation of p65 was analyzed in GIST-882 and GIST-T1 cells after KDM6A knockdown or SPARCL1 overexpression. $^{*}P < 0.05$ vs. control. $^{\#}P < 0.05$ vs. sh-KDM6A. **e, f** The expression of nuclear p65 was analyzed in GIST-882 and GIST-T1 cells after KDM6A knockdown or SPARCL1 overexpression. $^{*}P < 0.05$ vs. control. $^{\#}P < 0.05$ vs. sh-KDM6A.

after KDM6A knockdown and SPARCL1 overexpression reversed the stimulation induced by KDM6A knockdown in GIST-882 and GIST-T1 cells (Fig. 6c, d). Western blotting showed more p65 translocation to the nucleus after KDM6A knockdown. SPARCL1 overexpression reversed p65 translocation to the nucleus induced by KDM6A knockdown (Fig. 6e, f). These results indicate that p65 is a downstream effector of SPARCL1.

p65 is required for SPARCL1-induced angiogenesis in GIST

Tumour angiogenesis is vital for tumour growth and metastasis [28]. The p65 signaling pathway plays an important role in inflammatory cytokine and chemokine release [24, 29], involving angiogenic factors, such as VEGFA secreted by tumour cells. We next examined whether SPARCL1 was implicated in angiogenesis and the p65 inhibitor BAY11-7082 was selected for further study. SPARCL1 knockdown enhanced MMP9, LOX and VEGFA protein expression in GIST-882 and GIST-T1 cells. BAY11-7082 treatment decreased MMP9, LOX and VEGFA protein expression and recovered the acceleration induced by sh-SPARCL1 in GIST-882 and GIST-T1 cells (Fig. 7a–c). ELISA verified the observations of higher VEGFA after SPARCL1 knockdown, while BAY11-7082 showed the reverse observations (Fig. 7d). The conditioned media from GIST-882 or GIST-T1 cells with the indicated treatment were individually incubated with endothelial cells. Enhanced formation of tubes was observed in the sh-SPARCL1 group and BAY11-7082 inhibited the formation of tubes (Fig. 7e, f). In addition, both KDM6A and SPARCL1 expression was found to show a negative correlation with micro-vessel density and MMP9 expression in GIST tissues (Supplementary Fig. S4A-D), indicating that KDM6A and SPARCL1 were closely related to angiogenesis. Overall, our findings suggested that SPARCL1 is likely to be related to angiogenesis in GIST through accelerating p65 phosphorylation and nuclear translocation.

p65 participates in SPARCL1-mediated M2 polarisation and macrophage recruitment in GISTs

Tumour-associated macrophages (TAMs) are the primary components of the tumour microenvironment. Tumour cells secrete

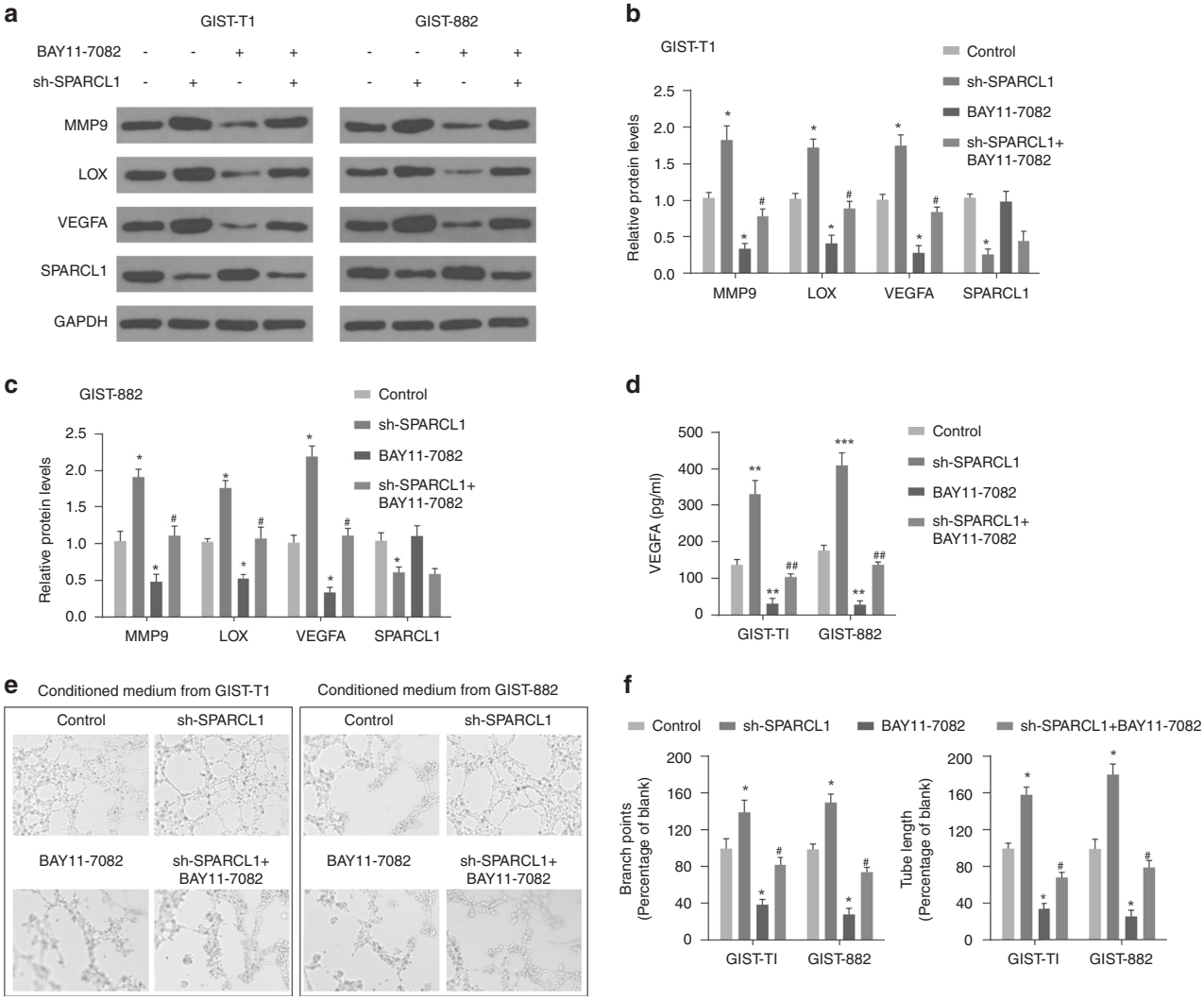

Fig. 7 p65 is required for SPARCL1-induced angiogenesis in GISTs. GIST-T1 and GIST-882 cells transfected sh-SPARCL1 were treated with 10 μmol/l BAY11-7082 for 1 h. **a–c** The expression of MMP9, LOX, VEGFA and SPARCL1 was analyzed in GIST-882 and GIST-T1 cells after the indicated treatment. $^{*}P < 0.05$ vs. control. $^{\#}P < 0.05$ vs. sh-SPARCL1. **d** The levels of VEGFA in conditional medium of GIST-882 and GIST-T1 cells after the indicated treatment were analyzed by ELISA. $^{**}P < 0.01$, $^{***}P < 0.001$ vs. control. $^{\#\#}P < 0.01$ vs. sh-SPARCL1. **e, f** Conditioned media from GIST-T1 or GIST-882 cells after the indicated treatment were incubated with HUVECs. Tube formation was examined based on the number of branching points and tube length per field. $^{*}P < 0.05$ vs. control. $^{\#}P < 0.05$ vs. sh-SPARCL1.

cytokines and chemokines to recruit monocytes to infiltrate cancer tissues and further promote M2-type polarisation. M2-like TAMs can in turn accelerate tumour growth, promote metastasis, and inhibit immune killing to promote tumour progression. The conditioned media from GIST-882 or GIST-T1 cells with the indicated treatment were individually incubated with THP-1 cells for 48 h. As shown in Fig. 8a and b, SPARCL1 inhibition enhanced the mRNA expression of M2 polarisation markers (CD206) and decreased the mRNA expression of M1 polarisation markers (CD86) in THP-1 cells. BAY11-7082 played the opposite roles. In addition, the flow cytometry results showed an enhancement in the percentage of CD206 + cells and a decrease in the percentage of CD86 + cells after SPARCL1 inhibition. However, BAY11-7082 decreased the percentage of CD206 + cells and increased the percentage of CD86 + cells (Supplementary Fig. S5A). Moreover, when macrophages were cocultured with the conditioned medium from SPARCL1 knockdown GIST cells, the motility of macrophages was significantly improved, indicating that SPARCL1 knockdown promoted the recruitment of macrophages (Fig. 8c). Importantly, the results of immunofluorescent staining indicated that more F4/80+ cells were found in sh-KDM6A xenografts and fewer F4/80+ cells were found in SPARCL1 xenografts (Fig. 8d). Moreover, CD206 + cells and CD86 + cells were separated from xenografts and counted by flow cytometry. The results indicated that more M2 macrophages and fewer M1 macrophages infiltrated cancer tissues, which further promoted the progression of GIST in the sh-KDM6A group. SPARCL1 overexpression had the opposite effect and recovered the change induced by sh-KDM6A (Supplementary Fig. S5B). In addition, both KDM6A and SPARCL1 expression in GIST tissues was found to be negatively related to the content of CD206 + cells (Supplementary Fig. S4E-F). BAY11-7082 treatment had no effect on tumour volume and tumour weight (Supplementary Fig. S5C-D). In summary, the KDM6A/SPARCL1/p65 axis is implicated in M2 polarisation and macrophage recruitment.

DISCUSSION

In this study, we found that KDM6A and SPARCL1 are downregulated in GISTs, while EZH2 is enhanced in GISTs. KDM6A and EZH2 regulate the transcription of SPARCL1 by demethylating histone H3 lysine trimethylation and consequently leads to inactivation of p65. The KDM6A-SPARCL1-p65 axis participates in

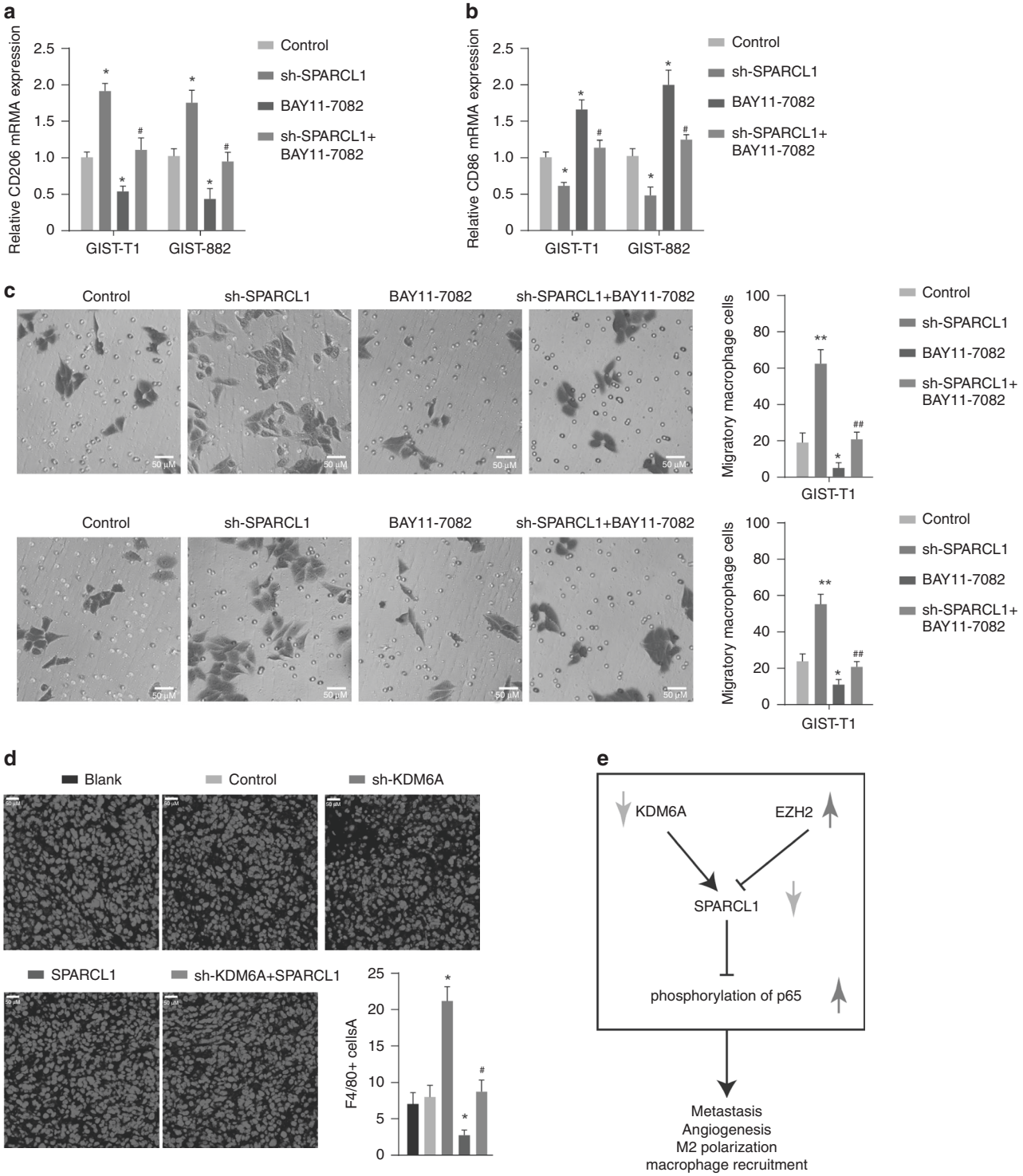

Fig. 8 SPARCL1 regulates M2 polarisation and macrophage recruitment via p65. GIST-T1 and GIST-882 cells transfected sh-SPARCL1 were treated with 10 μmol/l BAY11-7082 for 1 h. Then the conditioned media were collected and incubated with THP-1 cells for 24 h. **a, b** The mRNA expression of CD206 and CD68 in THP-1 cells was detected. $^{*}P < 0.05$ vs. control. $^{\#}P < 0.05$ vs. sh-SPARCL1. **c** THP-1 macrophage cells were added to the upper wells of a Boyden chamber, and GIST-T1 or GIST-882 cells were added to the lower chamber. THP-1 cells were allowed to migrate for 24 h at 37 °C before staining with crystal violet and quantification. $^{*}P < 0.05$, $^{**}P < 0.01$ vs. control. $^{\#\#}P < 0.01$ vs. sh-SPARCL1. **d** The infiltration of F4/80+ macrophages in xenografts was detected by immunofluorescent staining. $^{*}P < 0.05$ vs. control. $^{\#}P < 0.05$ vs. sh-SPARCL1. Data were displayed as the mean ± SEM. **e** Schematic model of the KDM6A-SPARCL1-p65 axis in regulating GIST.

angiogenesis, hepatic metastasis and macrophage infiltration in GISTs (Fig. 8e).

Metastasis is the leading cause of cancer death. Therefore, elucidating the driving mechanism of cancer metastasis is very important for the diagnosis, treatment and prognosis of cancer. High-risk GISTs are prone to metastasis and can easily grow from a small stromal tumour with the benign behaviour of a tumour with highly malignant biological behaviour [30–32]. In our study, we

found that KDM6A and SPARCL1 affected the migration and invasion of GIST cells in vitro and hepatic metastases in vivo. Mesenchymal-epithelial transition and matrix-metalloproteinases are closely related to tumour metastasis [24, 33, 34]. Furthermore, we verified that KDM6A and SPARCL1 affected the metastasis of GIST cells in a mesenchymal-epithelial transition- and matrix-metalloproteinases-dependent manner.

Studies have confirmed that p65 is abnormally activated in a variety of malignant tumours, and inhibition of p65 activity can inhibit the progression of a variety of tumours, suggesting that p65 plays an important role in the development of tumours [35–37]. p65 is an important transcription factor that directly or indirectly regulates the expression of inflammatory factors, cytokines, adhesion molecules, angiogenesis and anti-apoptotic molecules, thereby reshaping the tumour microenvironment and promoting the malignant progression of various tumours [38, 39]. The activation of the p65 pathway promotes the release of CCl2 from GIST cells and thus the recruitment of tumour-associated macrophages to further accelerate GIST malignancy [40]. In the present study, we found that SPARCL1 knockdown promoted the phosphorylation and nuclear translocation of p65, which may further alter the release of cytokines and promote angiogenesis, M2 polarisation and macrophage recruitment in GISTs.

The tumour microenvironment plays a crucial role in the process of tumour metastasis as the place where tumour cells live. The locally specific microenvironment might affect tumour progression at different sites [41]. GIST has varying immune cell infiltrate including tumour-associated macrophages [41–43]. Macrophage polarisation increases with tumour malignancy and has a prognostic value [44]. Tumour cells can release a variety of molecules to regulate different types of cells, and then transform the tumour microenvironment to further promote their malignant growth and metastasis [45, 46]. A predominance of the M2-phenotype macrophage population is found in GIST [43]. Chemokines in the tumour microenvironment can influence the recruitment and differentiation of macrophages [47]. For example, CCL2, which is associated with monocyte recruitment, transmigration and differentiation, is found to have the highest chemokine transcript expression in primary GISTs [41]. Mu et al. suggest that CCL2 upregulation causes recruitment of macrophages into the tumour leading to the tumour growth of GISTs [40]. KDM6A, SPARCL1 and p65 are closely related to the tumour microenvironment, but their functions in the GIST microenvironment need to be further verified. In our study, we confirmed that SPARCL1 affected macrophage polarisation and recruitment by changing the phosphorylation of p65. Both KDM6A and SPARCL1 influenced macrophage infiltration into cancer tissues in vivo. Moreover, the tumour microenvironment is also one of the main reasons for secondary imatinib resistance. Exploring the changes in the tumour microenvironment during the progression of GIST can also provide a new means to solve GIST drug resistance.

To summarise, this work outlines the involvement of the KDM6A-SPARCL1-p65 axis in the progression of GIST. KDM6A inhibits the metastasis and alters the microenvironment of tumours of GIST cells via demethylation at H3K27 at the SPARCL1 promoter, leading to the upregulation of SPARCL1 and the inactivation of p65. Overall, KDM6A and SPARCL1 may be potential therapeutic biomarkers for GIST.

DATA AVAILABILITY

The datasets used and/or analyzed during the current study are available from the corresponding authors on reasonable request.

REFERENCES

1. Blay JY, Kang YK, Nishida T, von Mehren M. Gastrointestinal stromal tumours. Nat Rev Dis Prim. 2021;7:22.
2. Joensuu H, Hohenberger P, Corless CL. Gastrointestinal stromal tumour. Lancet. 2013;382:973–83.
3. Al-Share B, Alloghbi A, Al Hallak MN, Uddin H, Azmi A, Mohammad RM, et al. Gastrointestinal stromal tumor: a review of current and emerging therapies. Cancer Metastasis Rev. 2021;40:625–41.
4. Brcic I, Argyropoulos A, Liegl-Atzwanger B. Update on molecular genetics of gastrointestinal stromal tumors. Diagnostics (Basel). 2021;11:194
5. Rubin BP, Blanke CD, Demetri GD, Dematteo RP, Fletcher CD, Goldblum JR, et al. Protocol for the examination of specimens from patients with gastrointestinal stromal tumor. Arch Pathol Lab Med. 2010;134:165–70.
6. Vallilas C, Sarantis P, Kyriazoglou A, Koustas E, Theocharis S, Papavassiliou AG, et al. Gastrointestinal stromal tumors (GISTs): novel therapeutic strategies with immunotherapy and small molecules. Int J Mol Sci. 2021;22:493.
7. Chen Z, Li S, Subramaniam S, Shyy JY, Chien S. Epigenetic regulation: a new frontier for biomedical engineers. Annu Rev Biomed Eng. 2017;19:195–219.
8. Lee MG, Villa R, Trojer P, Norman J, Yan KP, Reinberg D, et al. Demethylation of H3K27 regulates polycomb recruitment and H2A ubiquitination. Science. 2007;318:447–50.
9. Liu L, Cui J, Zhao Y, Liu X, Chen L, Xia Y, et al. KDM6A-ARHGDIB axis blocks metastasis of bladder cancer by inhibiting Rac1. Mol Cancer. 2021;20:77.
10. Xie G, Liu X, Zhang Y, Li W, Liu S, Chen Z, et al. UTX promotes hormonally responsive breast carcinogenesis through feed-forward transcription regulation with estrogen receptor. Oncogene. 2017;36:5497–511.
11. Kim JH, Sharma A, Dhar SS, Lee SH, Gu B, Chan CH, et al. UTX and MLL4 coordinately regulate transcriptional programs for cell proliferation and invasiveness in breast cancer cells. Cancer Res. 2014;74:1705–17.
12. Van der Meulen J, Sanghvi V, Mavrakis K, Durinck K, Fang F, Matthijssens F, et al. The H3K27me3 demethylase UTX is a gender-specific tumor suppressor in T-cell acute lymphoblastic leukemia. Blood. 2015;125:13–21.
13. Yi J, Shi X, Xuan Z, Wu J. Histone demethylase UTX/KDM6A enhances tumor immune cell recruitment, promotes differentiation and suppresses medulloblastoma. Cancer Lett. 2021;499:188–200.
14. Zhang C, Shen L, Zhu Y, Xu R, Deng Z, Liu X, et al. KDM6A promotes imatinib resistance through YY1-mediated transcriptional upregulation of TRKA independently of its demethylase activity in chronic myelogenous leukemia. Theranostics. 2021;11:2691–705.
15. Leng X, Wang J, An N, Wang X, Sun Y, Chen Z. Histone 3 lysine-27 demethylase KDM6A coordinates with KMT2B to play an oncogenic role in NSCLC by regulating H3K4me3. Oncogene. 2020;39:6468–79.
16. Girard JP, Springer TA. Cloning from purified high endothelial venule cells of hevin, a close relative of the antiadhesive extracellular matrix protein SPARC. Immunity. 1995;2:113–23.
17. Gagliardi F, Narayanan A, Mortini P. SPARCL1 a novel player in cancer biology. Crit Rev Oncol Hematol. 2017;109:63–8.
18. Hu H, Zhang H, Ge W, Liu X, Loera S, Chu P, et al. Secreted protein acidic and rich in cysteines-like 1 suppresses aggressiveness and predicts better survival in colorectal cancers. Clin Cancer Res. 2012;18:5438–48.
19. Hurley PJ, Marchionni L, Simons BW, Ross AE, Peskoe SB, Miller RM, et al. Secreted protein, acidic and rich in cysteine-like 1 (SPARCL1) is down regulated in aggressive prostate cancers and is prognostic for poor clinical outcome. Proc Natl Acad Sci USA. 2012;109:14977–82.
20. Hurley PJ, Hughes RM, Simons BW, Huang J, Miller RM, Shinder B, et al. Androgen-regulated SPARCL1 in the tumor microenvironment inhibits metastatic progression. Cancer Res. 2015;75:4322–34.
21. Naschberger E, Liebl A, Schellerer VS, Schutz M, Britzen-Laurent N, Kolbel P, et al. Matricellular protein SPARCL1 regulates tumor microenvironment-dependent endothelial cell heterogeneity in colorectal carcinoma. J Clin Invest. 2016;126:4187–204.
22. Shen C, Yin Y, Chen H, Wang R, Yin X, Cai Z, et al. Secreted protein acidic and rich in cysteine-like 1 suppresses metastasis in gastric stromal tumors. BMC Gastroenterol. 2018;18:105.
23. Yao D, Dai C, Peng S. Mechanism of the mesenchymal-epithelial transition and its relationship with metastatic tumor formation. Mol Cancer Res. 2011;9:1608–20.
24. Rozova VS, Anwer AG, Guller AE, Es HA, Khabir Z, Sokolova AI, et al. Machine learning reveals mesenchymal breast carcinoma cell adaptation in response to matrix stiffness. PLoS Comput Biol. 2021;17:e1009193.
25. Lan F, Bayliss PE, Rinn JL, Whetstine JR, Wang JK, Chen S, et al. A histone H3 lysine 27 demethylase regulates animal posterior development. Nature. 2007;449:689–94.
26. Hong S, Cho YW, Yu LR, Yu H, Veenstra TD, Ge K. Identification of JmjC domain-containing UTX and JMJD3 as histone H3 lysine 27 demethylases. Proc Natl Acad Sci USA. 2007;104:18439–44.
27. Ler LD, Ghosh S, Chai X, Thike AA, Heng HL, Siew EY, et al. Loss of tumor suppressor KDM6A amplifies PRC2-regulated transcriptional repression in bladder cancer and can be targeted through inhibition of EZH2. Sci Transl Med. 2017;9:eaai8312.
28. Versleijen-Jonkers YM, Vlenterie M, van de Luijtgaarden AC, van der Graaf WT. Anti-angiogenic therapy, a new player in the field of sarcoma treatment. Crit Rev Oncol Hematol. 2014;91:172–85.

29. Liu M, Xu W, Su M, Fan P. REC8 suppresses tumor angiogenesis by inhibition of NF-kappaB-mediated vascular endothelial growth factor expression in gastric cancer cells. Biol Res. 2020;53:41.
30. Hong AR, Yoon JH, Kim HK, Kang HC. Malignant prolactinoma with liver metastases masquerading as metastatic gastrointestinal stromal tumor: a case report and literature review. Front Endocrinol (Lausanne). 2020;11:451.
31. Yang J, Yan J, Zeng M, Wan W, Liu T, Xiao JR. Bone metastases of gastrointestinal stromal tumor: a review of published literature. Cancer Manag Res. 2020;12:1411–7.
32. Neppala P, Banerjee S, Fanta PT, Yerba M, Porras KA, Burgoyne AM, et al. Current management of succinate dehydrogenase-deficient gastrointestinal stromal tumors. Cancer Metastasis Rev. 2019;38:525–35.
33. Demirkan B. The roles of epithelial-to-mesenchymal transition (EMT) and mesenchymal-to-epithelial transition (MET) in breast cancer bone metastasis: potential targets for prevention and treatment. J Clin Med. 2013;2:264–82.
34. Xu L, Zheng Q. A novel expression signature from the perspective of mesenchymal-epithelial transition for hepatocellular carcinoma with regard to prognosis, clinicopathological features, immune cell infiltration, chemotherapeutic efficacy, and immunosuppressive molecules. J Oncol. 2021;2021:5033416.
35. Xia L, Tan S, Zhou Y, Lin J, Wang H, Oyang L, et al. Role of the NFkappaB-signaling pathway in cancer. Onco Targets Ther. 2018;11:2063–73.
36. Kabacaoglu D, Ruess DA, Ai J, Algul H. NF-kappaB/Rel transcription factors in pancreatic cancer: focusing on RelA, c-Rel, and RelB. Cancers (Basel). 2019;11:937.
37. Giuliani C, Bucci I, Napolitano G. The role of the transcription factor nuclear factor-kappa B in thyroid autoimmunity and cancer. Front Endocrinol (Lausanne). 2018;9:471.
38. Antonangeli F, Natalini A, Garassino MC, Sica A, Santoni A, Di Rosa F. Regulation of PD-L1 expression by NF-kappaB in cancer. Front Immunol. 2020;11:584626.
39. Betzler AC, Theodoraki MN, Schuler PJ, Doscher J, Laban S, Hoffmann TK, et al. NF-kappaB and its role in checkpoint control. Int J Mol Sci. 2020;21:3949.
40. Mu J, Sun P, Ma Z, Sun P. BRD4 promotes tumor progression and NF-kappaB/CCL2-dependent tumor-associated macrophage recruitment in GIST. Cell Death Dis. 2019;10:935.
41. Cameron S, Gieselmann M, Blaschke M, Ramadori G, Fuzesi L. Immune cells in primary and metastatic gastrointestinal stromal tumors (GIST). Int J Clin Exp Pathol. 2014;7:3563–79.
42. Cameron S, Haller F, Dudas J, Moriconi F, Gunawan B, Armbrust T, et al. Immune cells in primary gastrointestinal stromal tumors. Eur J Gastroenterol Hepatol. 2008;20:327–34.
43. van Dongen M, Savage ND, Jordanova ES, Briaire-de Bruijn IH, Walburg KV, Ottenhoff TH, et al. Anti-inflammatory M2 type macrophages characterize metastasized and tyrosine kinase inhibitor-treated gastrointestinal stromal tumors. Int J Cancer. 2010;127:899–909.
44. Mao X, Yang X, Chen X, Yu S, Yu S, Zhang B, et al. Single-cell transcriptome analysis revealed the heterogeneity and microenvironment of gastrointestinal stromal tumors. Cancer Sci. 2021;112:1262–74.
45. Zhou SL, Zhou ZJ, Hu ZQ, Huang XW, Wang Z, Chen EB, et al. Tumor-associated neutrophils recruit macrophages and T-regulatory cells to promote progression of hepatocellular carcinoma and resistance to sorafenib. Gastroenterology. 2016;150:1646–58.e17.
46. Ye H, Zhou Q, Zheng S, Li G, Lin Q, Wei L, et al. Tumor-associated macrophages promote progression and the Warburg effect via CCL18/NF-kB/VCAM-1 pathway in pancreatic ductal adenocarcinoma. Cell Death Dis. 2018;9:453.
47. Cavnar MJ, Zeng S, Kim TS, Sorenson EC, Ocuin LM, Balachandran VP, et al. KIT oncogene inhibition drives intratumoral macrophage M2 polarization. J Exp Med. 2013;210:2873–86.

AUTHOR CONTRIBUTIONS

LYH, BKL, GXZ and ZLC contributed to conceptualisation and methodology. BKL and XNY played a key role in interpreting the results and revised the article critically for important intellectual content. XNY and YY interpreted and analysed the data. CYS, ZXC and BZ designed the work that led to the submission, acquired data, revised the manuscript, acquired funding, supervised the project and agreed to be accountable for all aspects of the work in ensuring that questions related to the accuracy or integrity of any part of the work are appropriately investigated and resolved. All authors read and approved the final manuscript.

FUNDING

This work was supported by the Project of Science and Technology Department of Sichuan Province (No. 2020YFS0233).

COMPETING INTERESTS

The authors declare no competing interests.

ETHICS APPROVAL AND CONSENT TO PARTICIPATE

The study was conducted in accordance with the Declaration of Helsinki. The human tissues used in this study were approved by Committees for the Ethical Review of Research at the West China Hospital, Sichuan University. We have received consent from individual patients who have participated in this study.

CONSENT TO PUBLISH

Not applicable.

ADDITIONAL INFORMATION

Supplementary information The online version contains supplementary material available at https://doi.org/10.1038/s41416-022-01728-3.

Correspondence and requests for materials should be addressed to Bo Zhang.

Reprints and permission information is available at http://www.nature.com/reprints

Publisher's note Springer Nature remains neutral with regard to jurisdictional claims in published maps and institutional affiliations.